Journal of the Korean Magnetic Resonance Society **2021**, *25*, 39-44
DOI 10.6564/JKMRS.2021.25.3.039

Backbone assignment and structural analysis of anti-CRISPR AcrIF7 from *Pseudomonas aeruginosa* prophages

Iktae Kim[1,2] and Jeong-Yong Suh[1,*]

[1]Department of Agricultural Biotechnology and Research Institute of Agriculture and Life Sciences, Seoul National University, Seoul 08826, Republic of Korea
[2]Department of Biochemistry and Biophysics, Texas A&M University, College Station, TX 77843, United States

Received September 12, 2021; Revised September 18, 2021; Accepted September 18, 2021

Abstract The CRISPR-Cas system provides adaptive immunity for bacteria and archaea against invading phages and foreign plasmids. In the Class 1 CRISPR-Cas system, multi-subunit Cas proteins assemble with crRNA to bind to DNA targets. To disarm the bacterial defense system, bacteriophages evolved anti-CRISPR (Acr) proteins that actively inhibit the host CRISPR-Cas function. Here we report the backbone resonance assignments of AcrIF7 protein that inhibits the type I-F CRISPR-Cas system of *Pseudomonas aeruginosa* using triple-resonance nuclear magnetic resonance spectroscopy. We employed various computational methods to predict the structure and binding interface of AcrIF7, and assessed the model with experimental data. AcrIF7 binds to Cas8f protein via flexible loop regions to inhibit target DNA binding, suggesting that conformational heterogeneity is important for the Cas–Acr interaction.

Keywords AcrIF7, anti-CRISPR, chemical shifts, CRISPR-Cas

Introduction

Clustered regularly interspaced short palindromic repeats (CRISPRs) and CRISPR-associated (Cas) proteins constitute a variety of RNA-guided endonucleases that confer adaptive immunity on bacteria and archaea.[1–3] Upon infection, host bacteria employ the CRISPR-Cas system to integrate short fragments of invading nucleic acids as a spacer into the CRISPR loci. The CRISPR sequences are transcribed and processed into CRISPR RNAs (crRNAs) that guide Cas effector proteins to degrade foreign sequence upon subsequent invasion. The CRISPR-Cas systems are grouped into two classes based on the nature of the interference complex (multi-subunits or a single protein), and further divided into dozens of types and subtypes according to the phylogeny and targeting nucleic acids.[4] *Pseudomonas aeruginosa* possesses type I-C, I-E, and I-F CRISPR-Cas systems to fend off invading phages and plasmids. Among these, the type I-F CRIPSR-Cas system is comprised of a DNA-binding CASCADE complex and an effector Cas3 protein.[5] The CASCADE complex contains Cas5, Cas6, Cas8, and six Cas7 subunits that assemble with crRNA. Once the CASCADE complex recognizes and binds to the target sequence, the Cas3 nuclease is recruited to process both strands of target DNA in a progressive manner.

Bacteriophages have evolved different counter-

* Address correspondence to: **Jeong-Yong Suh,** Department of Agricultural Biotechnology and Research Institute of Agriculture and Life Sciences, Seoul National University, Seoul 08826, Republic of Korea. Tel: 82-2-880-4879; E-mail: jysuh@snu.ac.kr

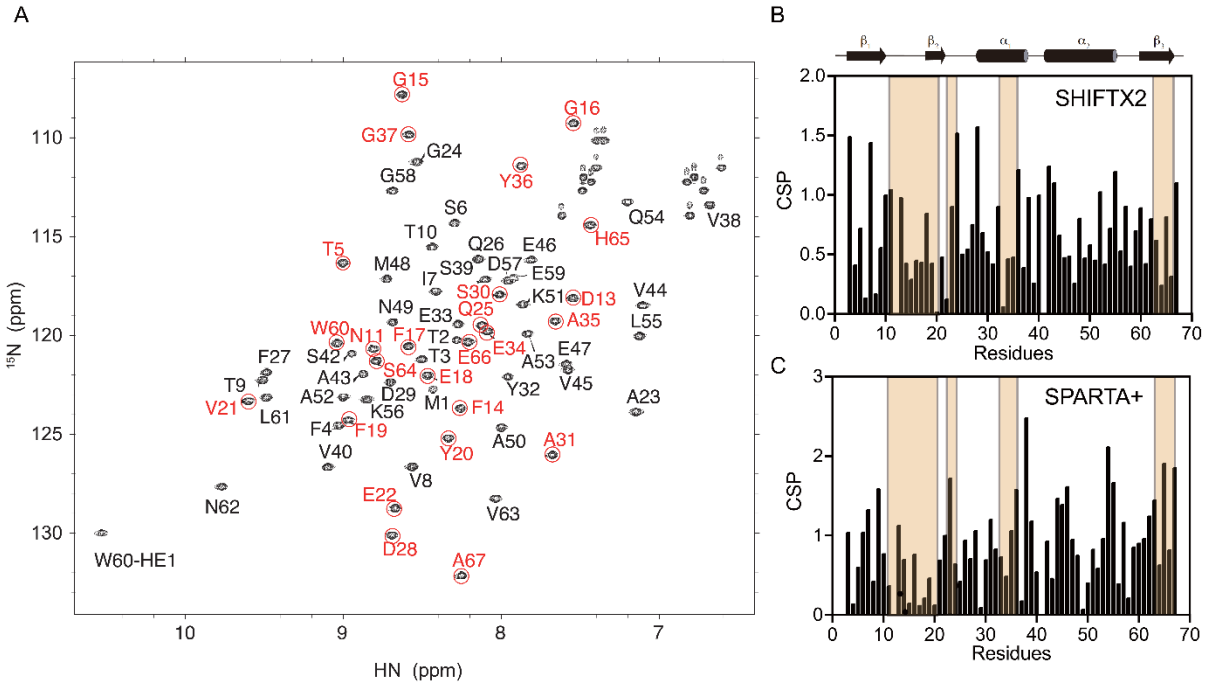

Figure 1. (A) ^{1}H-^{15}N HSQC spectrum of AcrIF7. The backbone amide resonances are annotated with the residue types and numbers. Residues at the binding interface for Cas8f are marked with red circles. Chemical shift perturbation plots from experimental shifts and those calculated by (B) SHIFTX2, and (C) SPARTA+. The binding interface of AcrIF7 for Cas8f are indicated with shaded boxes in orange.

defense mechanisms to neutralize the bacterial CRISPR-Cas machinery.[6] Among others, anti-CRISPR (Acr) proteins of phage origin directly inhibit the CRISPR-Cas function in host bacteria.[7–9] AcrIF7 first discovered in *P. aeruginosa* prophages effectively inhibits the type I-F CRISPR-Cas system of *P. aeruginosa*.[10] The structure and mechanism of AcrIF7 have been recently reported by NMR spectroscopy and cryogenic electron microscopy.[11,12] In this report, we describe the backbone assignment of AcrIF7 using the triple-resonance NMR spectroscopy. We also describe a comparative analysis of structures and interfaces obtained from popular prediction programs and experimental data.

Experimental Methods

Sample preparation- The synthetic AcrIF7 (a.a. 1–67) gene was cloned into a modified pET28a vector with an N-terminal His_6-tag and a maltose binding protein (MBP) tag followed by a tobacco etch virus (TEV) protease cleavage site. The plasmid was transformed into a BL21star(DE3) strain of *Escherichia coli* cells (Invitrogen), and the cells were grown in minimal media with $^{15}NH_4Cl$ and/or $^{13}C_6$-glucose as sole nitrogen or carbon sources, respectively. Cells were grown at 37°C until the optical density at 600 nm reached 0.6, induced with 0.5 mM isopropyl-β-D-thiogalactopyranoside at 17°C, and harvested by centrifugation after 16 hours of induction. Cell pellets were resuspended in 20 mM 4-(2-hydroxyethyl)-1-piperazineethanesulfonic acid (HEPES), pH 7.0, 300 mM NaCl, 5 mM β-mercaptoethanol (BME) and 10% (w/v) glycerol. After cell lysis using Emulsiflex and centrifugation, the supernatant was loaded onto a 5-ml HisTrap-HP column (GE Healthcare) pre-equilibrated with the binding buffer (20 mM HEPES, pH 7.0, 300 mM NaCl, 5 mM BME, 10% (w/v) glycerol and 30 mM imidazole). The column was washed with the same buffer, and a linear gradient of imidazole (up to 500 mM) was applied to elute the bound protein. The

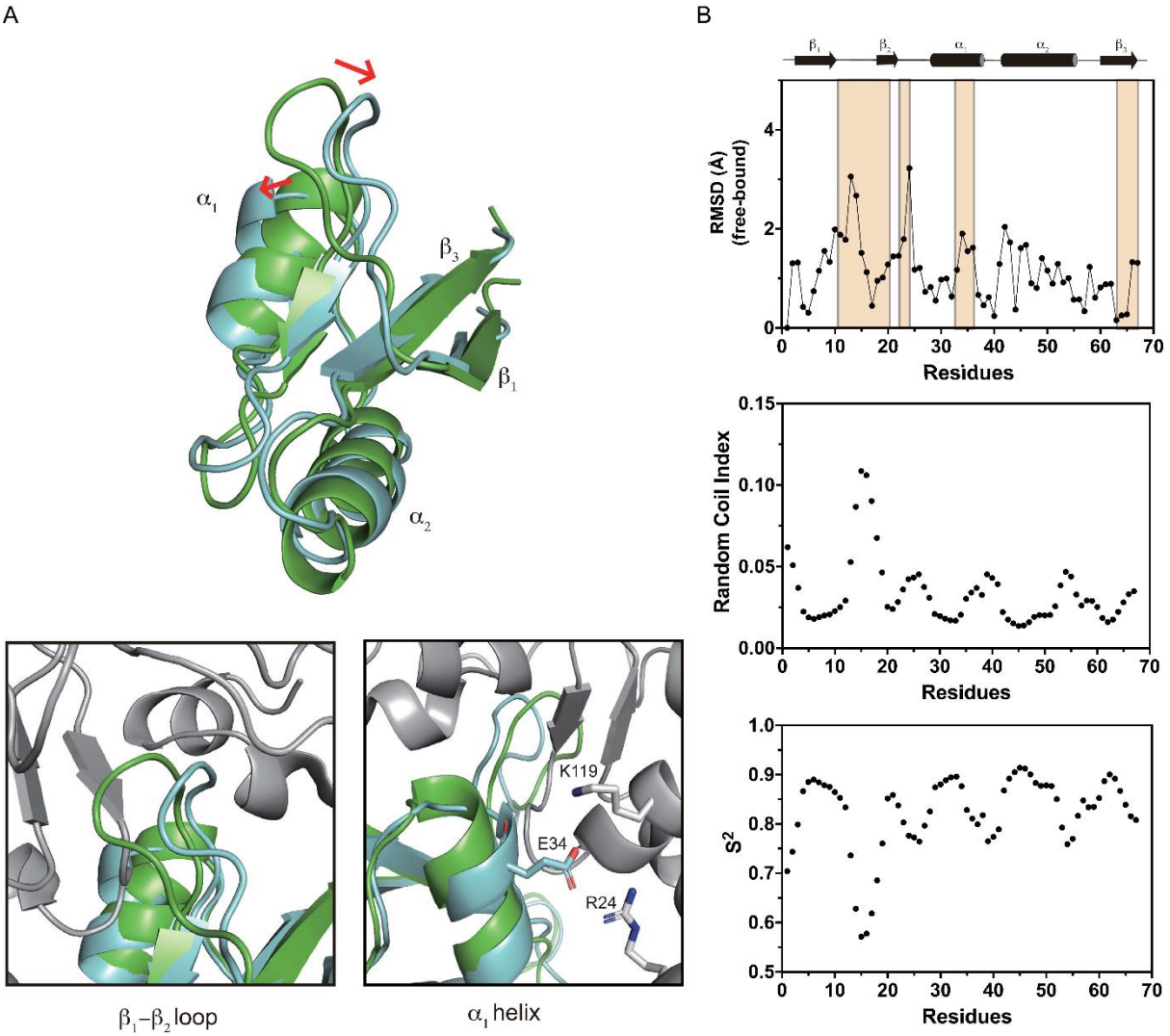

Figure 2. Conformational difference and dynamic property of AcrIF7. (A) Structural alignment of free AcrIF7 (PDB 6M3N, green) and AcrIF7 bound to Cas8f (PDB 7JZX, cyan). Changes in β1–β2 loop and α1 helix conformations upon binding of AcrIF7 and Cas8f are highlighted by red arrows in the top panel. Major conformational differences are shown in bottom panels with key residues involved in the binding shown as sticks. Cas8f is shown in gray. (B) Cα RMSD between the free and Cas8f-bound Acrf7 (top). The binding interface of AcrIF7 for Cas8f are indicated with shaded boxes in orange. The random coil index (middle) and order parameter (bottom) locate the dynamic regions as a function of residue number of AcrIF7.

N-terminal His_6-MBP tag was cleaved by TEV protease and separated by the HisTrap-HP column. Protein was further purified by the size-exclusion chromatography using a HiLoad 26/60 Superdex 75 column (GE Healthcare) equilibrated with buffer (20 mM HEPES, pH 7.0, 150 mM NaCl and 2 mM 1,4-dithiothreitol (DTT).

NMR experiments and data analysis- The NMR sample of 0.7 mM ^{13}C,^{15}N-AcrIF7 was prepared in 20 mM HEPES, pH 7.0, 150 mM NaCl, 2 mM DTT and 10% (v/v) D_2O. NMR spectra were recorded at 25°C on 800 and 900 MHz spectrometers equipped with a z-shielded gradient triple resonance probe. Sequential assignment of ^{1}H, ^{15}N and ^{13}C resonances were

achieved by three-dimensional triple resonance through-bond scalar correlation experiments CBCA(CO)NH, HNCACB, HNCO, HN(CA)CO, and HBHA(CO)NH. NMR spectra were processed using the NMRPipe,[13] and analyzed using NMRview and NMRFAM-Sparky programs.[14,15] Based on the experimental backbone chemical shifts, the backbone fold was predicted using a CS-Rosetta program.[16,17] Backbone random coil index (RCI) and order parameter were predicted using the TALOS+ program and the RCI web server.[18,19] Structures were displayed using the PyMOL software (The PyMOL Molecular Graphics System, Version 2.0 Schrödinger, LLC.).

Results and Discussion

Backbone assignment of AcrIF7- AcrIF7 (67 amino acids) exhibited a well dispersed 2D $^{1}H–^{15}N$ HSQC NMR spectrum typically observed in compact folded proteins (Figure 1A). We performed the sequential assignment of backbone ^{1}H, ^{15}N, and ^{13}C resonances of AcrIF7 using a combination of three-dimensional CBCA(CO)NH and HNCACB NMR experiments, and also HNCO and HN(CA)CO experiments.[20,21] The backbone chemical shifts were completely assigned except for the Cα resonance of Ser30 and the Cβ resonance of Ser42 that were absent in the CBCA(CO)NH and HNCACB spectra.

Based on the backbone chemical shifts, we initially attempted to generate a predicted backbone fold using the CS-Rosetta program. The predicted AcrIF7 fold exhibited a β-sheet with three β-strands with two flanking α-helices that were similar to our experimental structure. However, a closer examination revealed a distinct difference in the β-sheet topology. The experimentally determined structure of AcrIF7 adopted a β1-β3-β2 sheet (Figure 2A), whereas the CS-Rosetta program produced a β1-β2-β3 sheet. In addition, CS-Rosetta failed to locate the long loop between β1 and β2 strands that was important to the binding to the target Cas8f protein. This contrasts our previous study where the CS-Rosetta fold and the solution structure of AcrIIA4 agreed well in the three-dimensional topology of a β1-β2-β3 sheet[22,23]. It seems to us that the CS-Rosetta prediction have a preference toward sequential packing of β-strands.

In the complex structure of AcrIF7 and Cas8f, AcrIF7 blocks the DNA binding site of the Csy complex, competing with the protospacer adjacent motif of double-stranded target DNA. We attempted to calculate the amide resonance chemical shifts of AcrIF7 in complex with Cas8f using SHIFTX and SPARTA+ to assess the correlation of chemical shift perturbation and experimental binding interface.[24,25] SHIFTX predicts backbone and side chain chemical shifts based on empirical hypersurface approach combined with quantum mechanical calculations. SPARTA+ is a knowledge-based predictive method that calculates chemical shifts using analogous sequences and torsion angles in the public database. We calculated the chemical shifts of AcrIF7 in complex with Cas8f using both programs, and obtained chemical shift perturbation (CSP) of amide resonances by subtracting our experimental shifts of free AcrIF7. Neither of the calculated CSPs provided sufficient information on the binding interfaces, prompting a need for an improvement in the predictive parameters (Figures 1B and C).

Differences in structural coordinates upon Cas8f binding and dynamics of AcrIF7- We compared the free and Cas8f-bound AcrIF7 structures to examine whether AcrIF7 undergoes conformational changes upon binding to Cas8f in the Csy complex. The structural alignment indicated that AcrIF7 mostly maintained its $\beta_1\beta_2\alpha_1\alpha_2\beta_3$ fold of regular secondary structures regardless of Cas8f binding (Figure 2A). Notable conformational changes were observed in the β1–β2 loop region to avoid steric clash with Cas8f. The same loop also served a major binding interface for Cas8f, assisted by hydrogen bonds between Glu34 of AcrIF7 and *Arg24* and *Lys119* of Cas8f. We previously showed that Asp13 and Glu34 of AcrIF7 were important to Cas8f binding from mutagenesis combined with calorimetric measurements for binding affinity. Indeed, those residues participated in the binding interface via hydrogen bonds to *Arg24*, *Lys71*, and *Lys119* of Cas8f.[11,12]

The root-mean-square deviations of Cα positions between the free and Cas8f-bound AcrIF7 structures showed that the long β1–β2 linker loop (residues 10–

18) and the β2–α1 loop (residues 23–28) exhibited larger differences (rmsd > 2 Å) than the rest of the molecule (Figure 2B). We note that those residues with largest differences in the structural coordinates form the main binding interface for the Cas8f interaction. In order to find out whether the conformational changes are related to the dynamics of AcrIF7, random coil index (RCI) and predicted order parameter (S^2) of AcrIF7 were obtained from the chemical shift of AcrIF7. We note that the binding interface for Cas8f exhibits relatively high RCI and low S^2, indicating that the binding interfaces of AcrIF7 are dynamic and flexible. It has been reported that dynamic loop regions of AcrIIA4 also constitute the binding interfaces for type II-A Cas9.[20] It is interesting that the dynamic feature also appears at the end of the α1 helix (residue 35–37) that is part of the binding interface for Cas8f. We speculate the conformational plasticity of AcrIF7 may facilitate its target recognition and tight binding. Given that the sequences of those binding interfaces are well conserved among AcrIF7 homologs, we suppose that flexible loops play an important role for the AcrIF7–Cas8f interaction across different host strains.

In summary, we obtained the backbone chemical shifts of AcrIF7 using established strategies of sequential assignment, and employed the chemical shifts to investigate the conformations and dynamics of AcrIF7 via computational and experimental analysis. While AcrIF7 adopted a compact backbone fold, it was the dynamic regions that served as the binding interface for Cas8f to inhibit target DNA binding. Further analysis of backbone dynamics using relaxation parameters, and descriptions of μs-ms and ps-ns time-scale motions might provide useful information for understanding molecular mechanism of Acr proteins. Our finding suggests a link between dynamics and function of Acr proteins, which likely evolved during the arms race between phages and bacteria.

Acknowledgements

This work was supported by the Cooperative Research Program for Agriculture Science & Technology Development funded by Rural Development Administration (PJ01495901), the Creative-Pioneering Researchers Program through Seoul National University (500-20200255), and the Korea Basic Science Institute Program (C140440). We thank the high-field NMR facility at the Korea Basic Science Institute, and the National Center for Inter-University Research Facilities.

References

1. R. Jansen, J. D. v. Embden, W. Gaastra and L. M. Schouls, *Mol. Microbiol.* **43**, 1565 (2002).
2. R. Barrangou, C. Fremaux, H. Deveau, M. Richards, P. Boyaval, S. Moineau, D. A. Romero and P. Horvath, *Science* **315**, 1709 (2007).
3. S. J. Brouns, M. M. Jore, M. Lundgren, E. R. Westra, R. J. Slijkhuis, A. P. Snijders, M. J. Dickman, K. S. Makarova, E. V. Koonin and J. van der Oost, *Science* **321**, 960 (2008).
4. E. V. Koonin, K. S. Makarova and F. Zhang, *Curr. Opin. Microbiol.* **37**, 67 (2017).
5. K. S. Makarova, Y. I. Wolf, O. S. Alkhnbashi, F. Costa, S. A. Shah, S. J. Saunders, R. Barrangou, S. J. Brouns, E. Charpentier, D. H. Haft, P. Horvath, S. Moineau, F. J. Mojica, R. M. Terns, M. P. Terns, M. F. White, A. F. Yakunin, R. A. Garrett, J. van der Oost, R. Backofen and E. V. Koonin, *Nat. Rev. Microbiol.* **13**, 722 (2015).
6. J. E. Samson, A. H. Magadan, M. Sabri and S. Moineau, *Nat. Rev. Microbiol.* **11**, 675 (2013).
7. A. R. Davidson, W. T. Lu, S. Y. Stanley, J. Wang, M. Mejdani, C. N. Trost, B. T. Hicks, J. Lee and E. J. Sontheimer, *Annu. Rev. Biochem.* **89**, 309 (2020).

8. T. Wiegand, S. Karambelkar, J. Bondy-Denomy and B. Wiedenheft, *Annu. Rev. Microbiol*. **74**, 21 (2020).
9. N. Jia and D. J. Patel, *Nat. Rev. Mol. Cell Biol.* **22**, 563 (2021).
10. A. Pawluk, R. H. Staals, C. Taylor, B. N. Watson, S. Saha, P. C. Fineran, K. L. Maxwell and A. R. Davidson, *Nat. Microbiol.* **1**, 1 (2016).
11. I. Kim, J. Koo, S. Y. An, S. Hong, D. Ka, E.-H. Kim, E. Bae and J.-Y. Suh, *Nucleic Acids Res.* **48**, 9959 (2020).
12. C. Gabel, Z. Li, H. Zhang and L. Chang, *Nucleic Acids Res.* **49**, 584 (2021).
13. F. Delaglio, S. Grzesiek, G. W. Vuister, G. Zhu, J. Pfeifer and A. Bax, *J. Biomol. NMR* **6**, 277 (1995).
14. B. A. Johnson and R. A. Blevins, *J. Biomol. NMR* **4**, 603 (1994).
15. W. Lee, M. Tonelli and J. L. Markley, *Bioinformatics* **31**, 1325 (2015).
16. Y. Shen, O. Lange, F. Delaglio, P. Rossi, J. M. Aramini, G. Liu, A. Eletsky, Y. Wu, K. K. Singarapu and A. Lemak, *Proc. Natl. Acad. Sci. USA.* **105**, 4685 (2008).
17. O. F. Lange, P. Rossi, N. G. Sgourakis, Y. Song, H.-W. Lee, J. M. Aramini, A. Ertekin, R. Xiao, T. B. Acton and G. T. Montelione, *Proc. Natl. Acad. Sci. USA.* **109**, 10873 (2012).
18. Y. Shen, F. Delaglio, G. Cornilescu and A. Bax, *J. Biomol. NMR* **44**, 213 (2009).
19. M. V. Berjanskii and D. S. Wishart, *J. Am. Chem. Soc.* **127**, 14970 (2005).
20. B. Kim and J. H. Kim, *J. Kor. Magn. Reson. Soc.* **25**, 8 (2021).
21. D.-H. Kang, J.-J. Yi, D.-W. Sim, J.-W. Park, S.-H. Lee, E.-H. Kim, Y.-H. Jeon, W. S. Son, H.-S. Won and J.-H. Kim, *J. Kor. Magn. Reson. Soc.* **24**, 1 (2020).
22. I. Kim, M. Jeong, D. Ka, M. Han, N.-K. Kim, E. Bae and J.-Y. Suh, *Sci. Rep.* **8**, 1 (2018).
23. I. Kim, N.-K. Kim and J.-Y. Suh, *J. Kor. Magn. Reson. Soc.* **22**, 71 (2018).
24. S. Neal, A. M. Nip, H. Zhang and D. S. Wishart, *J. Biomol. NMR* **26**, 215 (2003).
25. Y. Shen and A. Bax, *J. Biomol. NMR* **38**, 289 (2007).